

Twisting attosecond pulse trains by amplitude-polarization IR pulsesEnrique G. Neyra ^{1,*}, Fabián Videla,^{2,3} Demian A. Biasetti,² Marcelo F. Ciappina ^{4,5,6,†} and Lorena Rebón ^{7,8,‡}¹*Instituto Balseiro (Universidad Nacional de Cuyo and Comisión Nacional de Energía Atómica) and CONICET CCT Patagonia Norte. Av. Bustillo 9500, Bariloche 8400 (RN), Argentina*²*Centro de Investigaciones Ópticas (CICBA-CONICET-UNLP), Cno. Parque Centenario y 506, P.O. Box 3, 1897 Gonnet, Argentina*³*Departamento de Ciencias Básicas, Facultad de Ingeniería UNLP, 1 y 47 La Plata, Argentina*⁴*Department of Physics, Guangdong Technion - Israel Institute of Technology, 241 Daxue Road, Shantou, Guangdong, 515063, China*⁵*Technion – Israel Institute of Technology, Haifa, 32000, Israel*⁶*Guangdong Provincial Key Laboratory of Materials and Technologies for Energy Conversion, Guangdong Technion - Israel Institute of Technology, 241 Daxue Road, Shantou, Guangdong, 515063, China*⁷*Departamento de Física, FCE, Universidad Nacional de La Plata, C.C. 67, 1900 La Plata, Argentina*⁸*Instituto de Física de La Plata, UNLP - CONICET, 1900 La Plata, Argentina*

(Received 10 July 2023; accepted 19 September 2023; published 5 October 2023)

Natively, atomic and molecular processes develop on a subfemtosecond timescale. In order to, for instance, track and capture the electron motion in that scale we need suitable “probes.” Attosecond pulses configure the most appropriate tools for such a purpose. These ultrashort bursts of light are generated when a strong laser field interacts with matter and high-order harmonics of the driving source are produced. In this work, we propose a way to twist attosecond pulse trains. In our scheme, each of the attosecond pulses in the train has a well-defined linear polarization, but with a different polarization angle between them. To achieve this goal, we consider an infrared pulse with a particular polarization state, called amplitude polarization. This kind of pulse was experimentally synthesized in previous works. Our twisted attosecond pulse train is then obtained by nonlinear driving an atomic system with that laser source, through the phenomenon of high-order harmonics generation. We achieve a considerable level of control over the modulation of the linear polarization state between two consecutive ultrashort bursts of extreme ultraviolet (XUV) radiation. Through quantum-mechanical simulations, supplemented with signal processing tools, we are able to dissect the underlying physics of the generation process. We are confident these polarized-sculpted XUV sources will play an instrumental role in future pump-probe-based experiments.

DOI: [10.1103/PhysRevA.108.043102](https://doi.org/10.1103/PhysRevA.108.043102)**I. INTRODUCTION**

Classical electrodynamics and quantum mechanics are the fundamental building blocks for the description of many natural phenomena. By measuring the wavelength and speed of light, electromagnetism provides us with tools to extract the velocity of the light field oscillations. Likewise, quantum mechanics links the rapidity of electronic motion with the energy distribution of the populated quantum states. By adequately tuning the light sources, these states can be accessed by photon absorption and emission. The native scale of both the light oscillations and electron dynamics falls within the attosecond range. These elementary processes comprise the constitutional steps of any change in the physical, chemical, and biological properties of materials and soft matter. The capability of capturing and manipulating them in real time is therefore relevant for the development of novel materials and technologies, as well as the understanding of fundamental atomic and molecular phenomena initiated by light fields [1,2].

Since the first measurement of an attosecond pulse train (APT) [3], attosecond science has grown enormously, from the obtaining of an isolate attosecond pulse (IAP) [4] to the generation of optical attosecond pulses [5], producing a great deal of applications based on these sources [6–8]. As is well known, APTs are obtained from the high-order harmonics generation (HHG) phenomenon. Here, a high-intensity infrared (IR) laser pulse interacts with a gaseous system producing, at every half laser cycle, a burst of extreme ultraviolet (XUV) radiation, i.e., a train of ultrashort XUV pulses is generated. The underlying physics behind the production of APT is rooted in the so-called three-step model, namely (i) tunneling ionization, (ii) classical motion, and (iii) recombination. The energy gained by the electron in its journey through the laser continuum is converted into a high-energy photon, upon recombination with the parent ion [9]. Full-blown quantum-mechanical models, based on the numerical solution of the time-dependent Schrödinger equation (TDSE) can be utilized as well, although the transparent link between the electron dynamics and their associated fundamental processes is lost.

The ability to obtain IAPs is key to exploring the electron dynamics in its natural timescale [4]. Although experimentally it is significantly more demanding to generate an IAP than an APT, different techniques, namely, amplitude gating,

*enriqueneyra@cnea.gob.ar

†marcelo.ciappina@gtiit.edu.cn

‡rebon@fisica.unlp.edu.ar

lighthouse, ionization gating, and distinct polarization gating setups [10,11], can be used to isolate a single attosecond pulse. On the other hand, manipulating the spatiotemporal properties or polarization state of laser pulses allows other degrees of freedom to be added to the laser-matter interaction beyond the frequency and amplitude of the radiation. To achieve this goal, there exists a great variety of pulse-shaping techniques [12–14] which require the use of optical elements and devices such as wave plates, spatial light modulators, acousto-optic modulators, and interferometer systems that can work in the visible and IR region of the electromagnetic spectrum. However, to have control of the XUV coherent radiation as in the visible-IR region is highly challenging because, in general, there are no simple physical devices designed for that wavelength range. Therefore, the control of the different properties of the coherent XUV radiation generated via HHG should come from the manipulation of the IR driving pulse.

Several schemes and sources have been used so far, that allows a high degree of control in the produced XUV radiation, e.g., attosecond light vortices [15,16], structured light beams carrying optical angular momentum (OAM) [17], controlled OAM sources [18,19], chirality in nonlinear optics [20], and others [21,22]. In particular, by using bichromatic and counter-rotating circularly polarized pulses, it is possible to generate high-order harmonics with circular polarization, in a gaseous medium [23–26]. In the temporal domain, such harmonics originate an APT where the polarization state of each attosecond pulse depends on the Lissajous curves that describe the bichromatic driving field, where these curves are shaped like a flower whose petals are distributed equidistantly on a circumference [25,27–32]. Moreover, the temporal structure of these attosecond pulses has a period that depends on the frequency ratio in the bichromatic field. Such a ratio also gives the number of petals in the Lissajous curves and the angle between them. This possibility of manipulating the polarization state of each attosecond pulse in the APT allows for a more sophisticated level of development and understanding of ultrafast magnetism [33,34] in the XUV region, both in molecules [35] and in solid systems [36]. In addition, it enables the exploration of chiral systems [37] and the tomographic reconstruction of circularly polarized high-harmonics fields [38].

In this contribution, we study the HHG in a gaseous target driven by two single-color orthogonal polarized pulses, which are time delayed from each other. We model the nonlinear laser-matter electron dynamics through the numerical solution of the three-dimensional time-dependent Schrödinger equation (3D-TDSE) in the single-active-electron approximation. We further analyze the properties in the polarization of the generated APT as well as its temporal anatomy by invoking signal processing tools. We show a procedure to twist the APT, obtaining a different behavior from that which can be obtained from previous techniques. As a result, each of the attosecond pulses in the train has a well-defined linear polarization, but with a different polarization angle between them. Our technique has the advantage of using a simpler experimental setup, since only a single-color driving pulse is needed. In the temporal domain, our technique to generate the synthesized polarization pulse, can resemble the generation of an APT using counter-rotating circularly polarized pulses

of two different frequencies. Nonetheless, when considering the spectral domain, these two techniques display notable differences.

II. AMPLITUDE-POLARIZED PULSES

When a linearly polarized laser pulse with an electric field $\mathbf{E}(t)$, carrier frequency ω_0 , field envelope $f(t)$ and global phase ϕ , incident upon a birefringent medium with its polarization direction to a given angle with respect to the optical axis, the field components $E_x(t)$ and $E_y(t)$ travel with different velocities in such a medium. Thus, a temporal delay τ is generated between them. In particular, for a polarization direction at an angle of 45° , this field can be mathematically described as $\mathbf{E}(t) = E_x(t)\check{e}_x + E_y(t)\check{e}_y = E_0 f(t)\cos(\omega_0 t + \phi_x)\check{e}_x + E_0 f(t - \tau)\cos(\omega_0 t + \phi_y)\check{e}_y$, where E_0 is the laser electric-field peak amplitude, and the phases ϕ_x and ϕ_y take into account the global phase of the field ϕ . In general, when the phase difference $\Delta\phi = \phi_y - \phi_x = -\omega_0\tau \neq n\pi$ ($n \in \mathbf{Z}$), it is said that the pulse has circular ($\Delta\phi = \pm\pi/2$) or elliptical (any other value of $\Delta\phi$) polarization, with ellipticity $\epsilon = 1$ ($0 < \epsilon < 1$) for circular (elliptical) polarization. It should be noted that, in the considered case ($\Delta\phi \neq n\pi$), the pulse has a time-dependent ellipticity $\epsilon(t)$, since the field envelope has a temporal delay τ . One question immediately arises: How fast is it the variation of $\epsilon(t)$? The answer can be formulated as follows: given that $\epsilon(t)$ depends on the bandwidth of the pulse $\Delta\omega$, the variation will be fast or slow depending on whether $\Delta\omega \approx \omega_0$ or $\Delta\omega \ll \omega_0$, respectively.

On the other hand, when the phase difference is $\Delta\phi = n\pi$, the mathematical description of the field results in $\mathbf{E}(t) = E_0 f(t)\cos(\omega_0 t + \phi)\check{e}_x + E_0 f(t - \tau)\cos(\omega_0 t + n\pi + \phi)\check{e}_y = E_0(f(t)\check{e}_x + f(t - \tau)\check{e}_y)\cos(\omega_0 t + \phi)$, with n even, and $\mathbf{E}(t) = E_0(f(t)\check{e}_x - f(t - \tau)\check{e}_y)\cos(\omega_0 t + \phi)$ if n is odd. It is worth mentioning that the electric field must be written in this way because the pulse has a bandwidth $\Delta\omega \neq 0$. Contrariwise, for a monochromatic field, a temporal translation $\tau = n\pi/\omega_0$ does not change the amplitude ratio between the two orthogonal polarizations.

Experimentally, the polarization scheme described above was presented and synthesized in Ref. [39] to control the angular-momentum orientation of N_2 molecules. Later on, other molecular scenarios were studied [40–45]. This polarization deserves a different classification from linear, circular, or elliptical and, taking into account its mathematical expression, we call it *amplitude polarization* (AP). However, its denomination is not unified in the literature, and different authors refer to it in different ways, namely, unidirectional polarization [41], twisted polarization [40], polarization-shaped pulse [42], and polarization-skewed [43,46].

In what follows, we show how this AP field can be used to twist an APT. In Fig. 1, it can be seen a schematic representation of the experimental setup necessary to obtain the AP pulses and, through the HHG in a gaseous system, the twisted APT. First, the IR-AP pulse is generated by a multiple-order wave plate (MOWP) and a Berek compensator (BC), which are placed in the path of a single beam, linearly polarized at 45° with respect to the optical axis of the MOWP [39]. This configuration presents a substantial advantage over other polarization synthesis schemes for the generation or

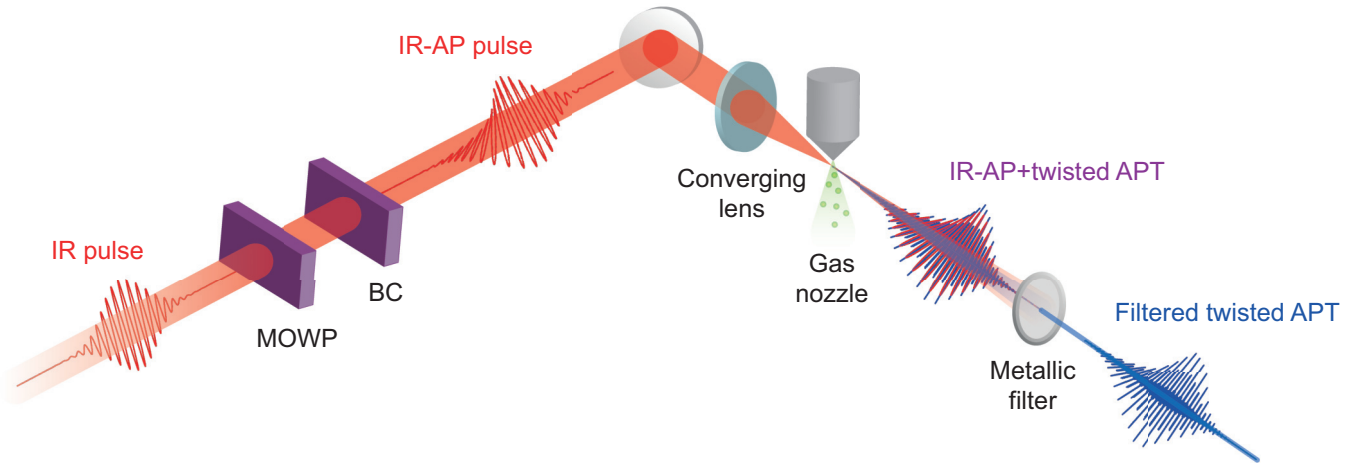


FIG. 1. Schematic representation of the experimental setup. The IR–AP pulse is generated by a multiple-order wave plate (MOWP) and a Berek compensator (BC). These two optical elements are placed in the path of a single beam. The input IR pulse is linearly polarized at 45° with respect to the optical axis of the MOWP. The synthesized IR–AP pulse crosses a supersonic atomic gas jet, and high-order harmonics are generated, whose polarization is controlled by the properties of the IR–AP field. The resulting twisted APT is then filtered and it can be used to study elementary atomic or molecular processes in its natural timescale.

manipulation of attosecond pulses, where two-color pulses and a complex interferometric system are required [25,27–29,36,38]. In our proposal, the previously synthesized IR–AP pulse crosses a supersonic gas jet and high-order harmonics are generated whose polarization is sculpted by the properties of the IR–AP field. The resulting APT, after appropriate filtering, can then be used to drive an atomic, molecular, or solid sample, and track the multidimensional electron dynamics with attosecond time resolution.

III. TWISTED ATTOSECOND PULSE TRAINS

Our aim here is to understand the underlying physics of the interaction of the IR–AP pulses with an atomic target. To this end, we compute the HHG spectra for different values of the relevant field parameters, on a prototypical atomic system.

We can start by defining the AP electric field $\mathbf{E}(t)$ through the explicit expressions of its components $E_x(t)$ and $E_y(t)$. For instance, assuming a Gaussian field envelope $f(t)$, they are written as

$$E_x(t) = E_0 e^{-2 \ln(2) \left(\frac{t+\tau/2}{\Delta t}\right)^2} \cos[\omega_0(t + \tau/2) + \phi], \quad (1a)$$

$$E_y(t) = E_0 e^{-2 \ln(2) \left(\frac{t-\tau/2}{\Delta t}\right)^2} \cos[\omega_0(t - \tau/2) + \phi], \quad (1b)$$

where Δt is the temporal full width at half maximum (FWHM). For simplicity, the temporal delay τ is expressed symmetrically around $t = 0$.

Based on the expressions in Eqs. (1a) and (1b), our numerical calculations were performed for a value $E_0 = 0.053$ a.u., corresponding to a laser intensity $I_0 = 10^{14}$ W/cm², and a wavelength $\lambda = 800$ nm ($\omega_0 = 0.057$ a.u.). We have analyzed the interaction between the IR–AP pulses both in the multi- and few-cycle regimes. For the first case, we considered pulses with a FWHM of $\Delta t = 5$ optical cycles (1 optical cycle = $2\pi/\omega_0 \approx 2.7$ fs). For the second one, we have set the FWHM to $\Delta t = 2$ optical cycles. By means of the

3D–TDSE in the single active electron (SAE) approximation (see Refs. [47,48] for details), we computed the x and y components of the HHG spectrum, driven by $\mathbf{E}(t)$. As a prototypical atomic target, we consider hydrogen (H), with an ionization potential $I_p = 0.5$ a.u. Any other atomic target can be adequately modeled by tuning the parameters of the associated model potential. The temporal delay τ is chosen to be $\tau = \Delta t$. For this choice, the peak strength of the synthesized AP field, $|\mathbf{E}(t)|_{\max}$, remains almost constant and equal to E_0 , in the central region of the pulse (see Appendix A).

In Fig. 2 we show the results obtained by the 3D–TDSE for an AP pulse with a temporal FWHM of $\Delta t = 5$ optical cycles and a global phase $\phi = 0$. Figures 2(a) and 2(b) show the projection of the harmonic radiation in the x and y axes, respectively (see Appendix B). Meanwhile, Figs. 2(c) and 2(d) depict the time-frequency representation (wavelet analysis) of the above-cited spectra and, superimposed, the respective electric-field components $E_x(t)$ (white line) and $E_y(t)$ (gray line).

The core of our results is shown in Fig. 3, where the temporal structure of the twisted APT can be seen. This temporal representation was obtained after spectrally filtering the HHG of Figs. 2(a) and 2(b) above the 20th harmonic. Then, only the regions of the spectrum colored in red (right regions) in Figs. 2(a) and 2(b) are considered, which in turn correspond to the region above the horizontal black line in Figs. 2(c) and 2(d). It should be noted that, experimentally, a Si filter can be used in this spectral range [49]. This spectral filtering allows us to select the so-called cutoff region, where the spectral phase of the harmonics is almost constant and the respective attosecond pulses are nearly Fourier-limited. On the contrary, it is well known that in the plateau region of the HHG spectrum, due to the different recombination times of different electron trajectories, i.e., different emission times of the radiation [see the wavelet analysis in Figs. 2(c) and 2(d)], the generation of the attosecond pulses has an intrinsically spectral phase, the so-called attochirp. In general, this phase

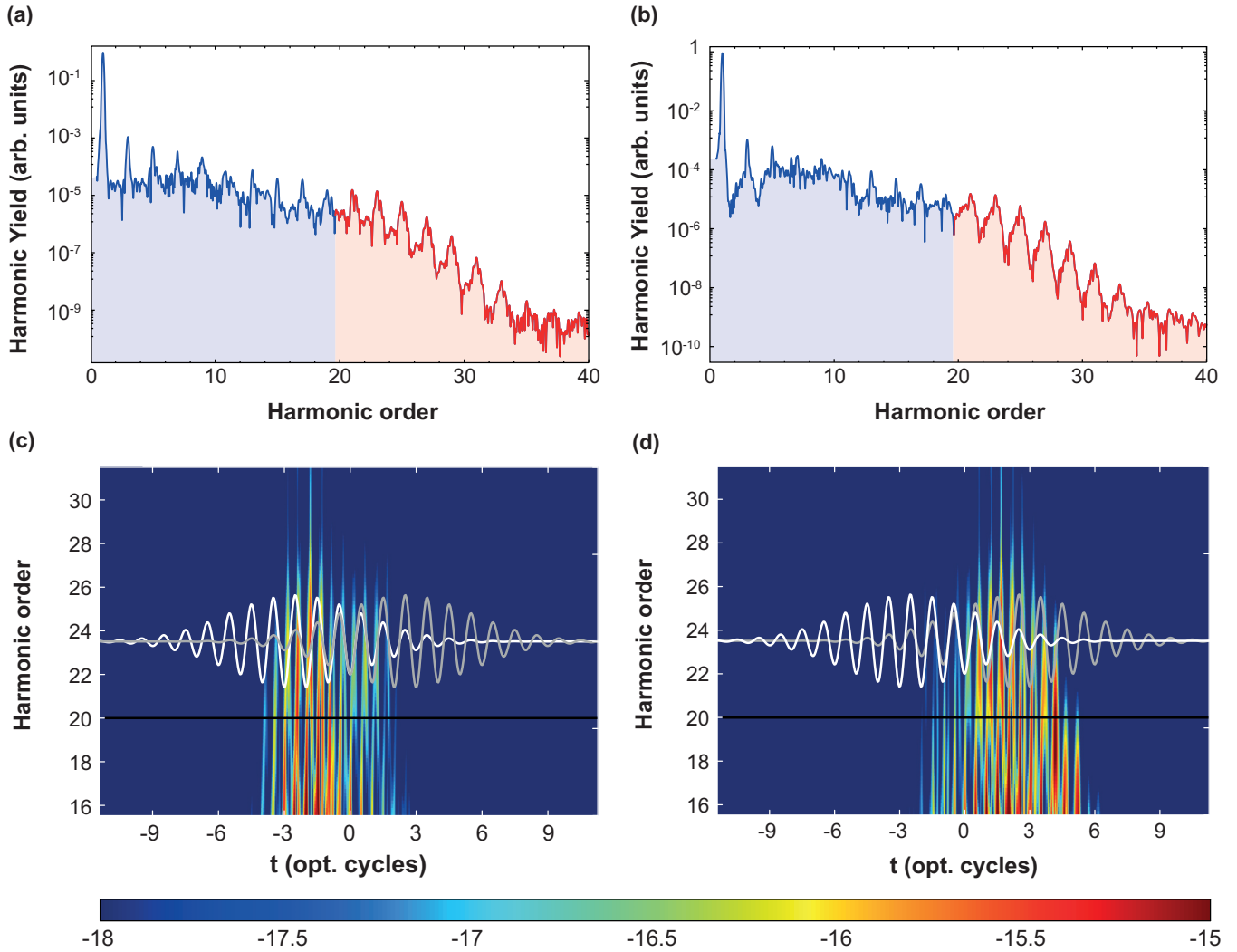


FIG. 2. High-order harmonic generation driven by amplitude-polarization (AP) multicycle pulses. (a), (b) HHG spectra generated by the field components $E_x(t)$ and $E_y(t)$, respectively. The FWHM of the AP pulse is $\Delta t = 5$ optical cycles and the global phase is $\phi = 0$. The red regions in the spectra represent the portion selected to obtain the twisted APTs (see text for details). (c), (d) Wavelet analysis (see Appendix B) obtained from the dipole accelerations $a_x(t)$ and $a_y(t)$, respectively. The color maps indicate the value of the corresponding Gabor transform (in log scale) as a function of time and harmonic order. The x (y) component of the AP pulse is superimposed with a white (gray) solid line (advanced and delayed components, respectively). The black solid line at the 20th harmonic defines the lower limit of the selected spectral region.

can be experimentally compensated by a metallic foil [50]. Also, it is worth mentioning that it is possible to tune the cutoff region by manipulating the laser intensity I or wavelength λ of the driving field (the harmonic cutoff scales as $I\lambda^2$), to overlap the spectral region with the spectral response of other filters, such as Al or Zr [49].

Let us now aim to dissect the twisted temporal anatomy of the APT. For this purpose we have plotted, in Fig. 3(a), the components of the field $\mathbf{E}(t)$ (dashed lines) and the twisted APT (solid lines). The x components (y components) are shown in red (blue) color (advanced and delayed components, respectively). From there, it can be seen that the attosecond pulses are generated every half cycle of the AP pulse and, what is most important, the relative amplitude between the x and y components of the attosecond pulses in the train, changes from one pulse to the next. This indicates that the

polarization between two adjacent attosecond pulses is different. Furthermore, the full temporal 3D representation of the twisted APT can be seen in Fig. 3(b) (thin blue line), where we have also included the laser electric field of the AP pulse (thick red line). From this figure, the temporal evolution of each attosecond pulse polarization in the train and how it rotates is clearly observed by following the temporal evolution of the AP pulse.

For a better visualization of the polarization features of the individual attosecond pulses, in Fig. 3(c) we show the Lissajous curves of both, the laser electric field of the AP pulse (thick red line) and the electric field of the twisted APT (thin blue line). Two key observations can be extracted from this figure: First, each attosecond pulse has almost perfect linear polarization. Second, the polarization direction of each attosecond pulse follows the orientation of the “petals,” which

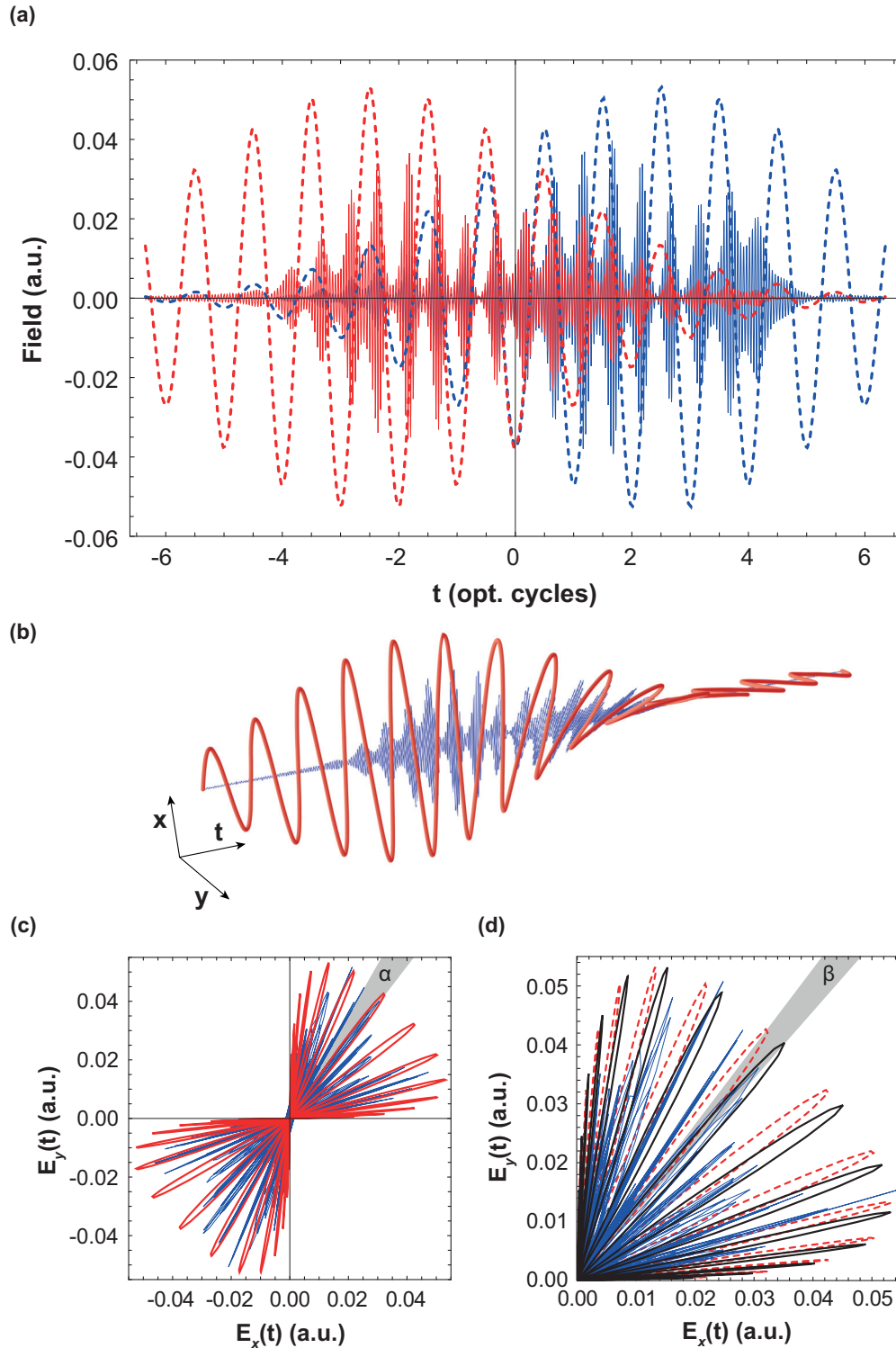


FIG. 3. Temporal anatomy of the twisted APT: multicycle pulses regime. (a) Projection of the twisted APT in the x and y directions (red and blue solid lines, respectively) and the field components $E_x(t)$ and $E_y(t)$ of the AP pulse (red and blue dashed lines, respectively). In both cases, the x and y components are the advanced and delayed components, respectively. These results correspond to those of Fig. 2, in the selected region of the spectra [right regions, colored in red, in Figs. 2(a) and 2(b)]. (b) A 3D representation of the twisted APT (thin blue line) and the laser electric field of the AP pulse (thick red line). (c) Lissajous figures of the laser electric field of the AP pulse (thick red line) and the twisted APT (thin blue line). The gray shadow region depicts the angular spacing α , between the polarization direction of two adjacent attosecond pulses. (d) Same as panel (c) but for a driving AP field with a global phase $\phi = \pi/2$ (black solid line, plotted only in the first quadrant). Here, the laser electric field of the AP pulse with a global phase $\phi = 0$ is also shown (red dashed line). Here, the gray shadow region depicts the angular spacing β , between the polarization direction of the two AP pulses.

describe the polarization of the AP electric field. It is possible to obtain the difference in the polarization direction between two adjacent attosecond pulses, accounted by α (see the gray shadowed region), which in this case is $\approx 7.5^\circ$.

Finally, from Fig. 3(d), we can analyze how the previous results vary by changing the global phase of the driving AP pulse by $\pi/2$. Considering that the polarization direction of the attosecond pulses is given by the position of the petals, for a clear comparison, we show the Lissajous curves of the electric fields only in the first quadrant. Here, an AP pulse with global phase $\phi = 0$ ($\phi = \pi/2$) is represented by a dashed red (solid black) line, while the twisted APT is depicted by a thin blue solid line. The change in the polarization direction between these AP fields, with different global phases, is indicated as β (see the gray shadowed region).

Since the direction of the electric-field vector of each attosecond pulse follows the orientation of the petals that describe the polarization of the AP field, the APT rotates, globally, at an angle equal to β . In this case $\beta \approx 3.9^\circ$, i.e., $\beta \approx \alpha/2$, which is a general result when $\phi \rightarrow \phi \pm \pi/2$. If ϕ is changed by a different value, the relation between β and α will be different.

All the analysis presented above was made in the multi-cycle regime. To complete the picture, in the following we examine the dynamics for a few-cycle AP pulse. While the physics is the same for both the multi- and few-cycle regimes, the quantitatively and/or qualitatively characteristics of the resulting APT are not the same. The study of both example cases allows a clearer understanding of the technique to synthesize the driving AP pulse, and its effects on the HHG, i.e., how do we use the bandwidth of the AP pulse $\Delta\omega$, or equivalently its temporal FWHM Δt , to create a twisted APT with controllable linear polarization.

In Fig. 4 we show our results for an AP pulse with a FWHM of $\Delta t = 2$ optical cycles. For this FWHM, the angular spacing between two adjacent petals in the AP pulse is significantly larger than in the previous multicycle case. To make a one-to-one comparison, in Figs. 4(a) and 4(b) we show the wavelet analysis coming from the associated HHG spectra in this few-cycle instance. The x and y components of the AP electric field $\mathbf{E}(t)$ are superimposed in white and gray solid lines, respectively. Likewise, in Fig. 4(c) we plot both the electric-field components of the AP field (dashed line) and the APT (solid line). Here, the x components (y components) are shown in red (blue) color (advanced and delayed components, respectively). As in the previous case, the relative amplitude between the components of the attosecond pulses changes from one pulse to the next. From the Lissajous curve [Fig. 4(d)] a slightly greater ellipticity of the attosecond pulses is observed in relation to that observed Fig. 3(d), and a larger angle α between the polarization direction of two adjacent pulses ($\alpha \approx 20^\circ$). The full temporal evolution of the twisted APT is then shown in Fig. 4(e). As in the multicycle regime, the HHG spectra were spectrally filtered, and we depicted here only from the 20th-harmonic onwards [see the horizontal black line in Figs. 4(a) and 4(b)].

A more detailed analysis of the angle α as a function of the temporal FWHM Δt , and the time delay τ , can be found in Appendix C. Here, in Fig. 5, we show such a value for each of the two AP pulses considered in this work. Top red

(bottom blue) circles represent the case of $\Delta t = 2$ ($\Delta t = 5$) optical cycles, while the corresponding linear approximation, given by $\alpha_1(\tau, \Delta t) = \ln(2)\tau/\Delta t^2$, is indicated by the top red (bottom blue) triangles. It is observed that α has a linear-like behavior as a function of the delay τ , in the case of $\Delta t = 5$ optical cycles. For $\Delta t = 2$ optical cycles the linearity holds, approximately, until $\tau \approx 2$ optical cycles. As a summary, we can say that the expression $\alpha_1(\tau, \Delta t)$ gives a precise understanding of how to manipulate the change in the polarization direction between two adjacent attosecond pulses, from the synthesis of the driving IR field. Furthermore, the calculation of the recollision angles of the ionized electrons [47] are included in Appendix D.

It is important to note that all the presented results are based on the numerical solution of the 3D-TDSE, i.e., our analysis corresponds to the single-atom response. A macroscopic study, which exceeds the focus of the present work, is necessary for a more general analysis of the phenomenon. Nevertheless, since the AP driving pulses have a polarization state that is slightly different from that of a linearly polarized pulse, we do not see, in principle, major drawbacks in the use of those pulses for HHG when, for example, the role of harmonic phase-matching condition would be important. Even more, bichromatic counter-rotating circularly polarized pulses, with a more complex synthesis than the AP pulses, were already used for HHG in real experimental conditions, within a wide range of laser parameters (see, for example, Refs. [25,35]). Therefore, we think that there should be no special considerations to take into account in that regard.

IV. DISCUSSION

In this work, we have introduced a straightforward procedure to generate an APT in which each of the attosecond pulses has a well-defined linear polarization that differs between pulses. This appealing feature of the APT is achieved through the manipulation of the polarization state of the driving IR field. Here, by introducing a variable time delay between two identical copies of an IR pulse, we obtain an AP pulse. Classically speaking, the generation of this twisted APT is rooted in the small deviation of the trajectories of the electrons in the continuum by the AP pulse, due to the temporal change in its polarization state. This makes the electrons recombine at different angles, where the “short” trajectories slightly deviate in relation to the “long” ones. Furthermore, this deviation is more pronounced with few-cycle driving pulses, which allows for reaching larger rotation angles. Thus, this small deviation of the electrons’ trajectories in relation to the linear polarization pulse, allows us to extend the current results by employing different conventional sources to obtain an APT, such as high-energy laser sources, at a high repetition rate, or with different wavelengths. Moreover, our scheme is quite versatile and robust, as it can be implemented in both the multi- and few-cycle regimes.

The concrete possibility to manipulate the polarization angle between the attosecond pulses in the APT would bring new perspectives to the current attosecond-based spectroscopy techniques [51–55]. For instance, it would be possible to generate photoelectrons within a well-defined angular range or design complex pump-probe techniques. Just to cite a few

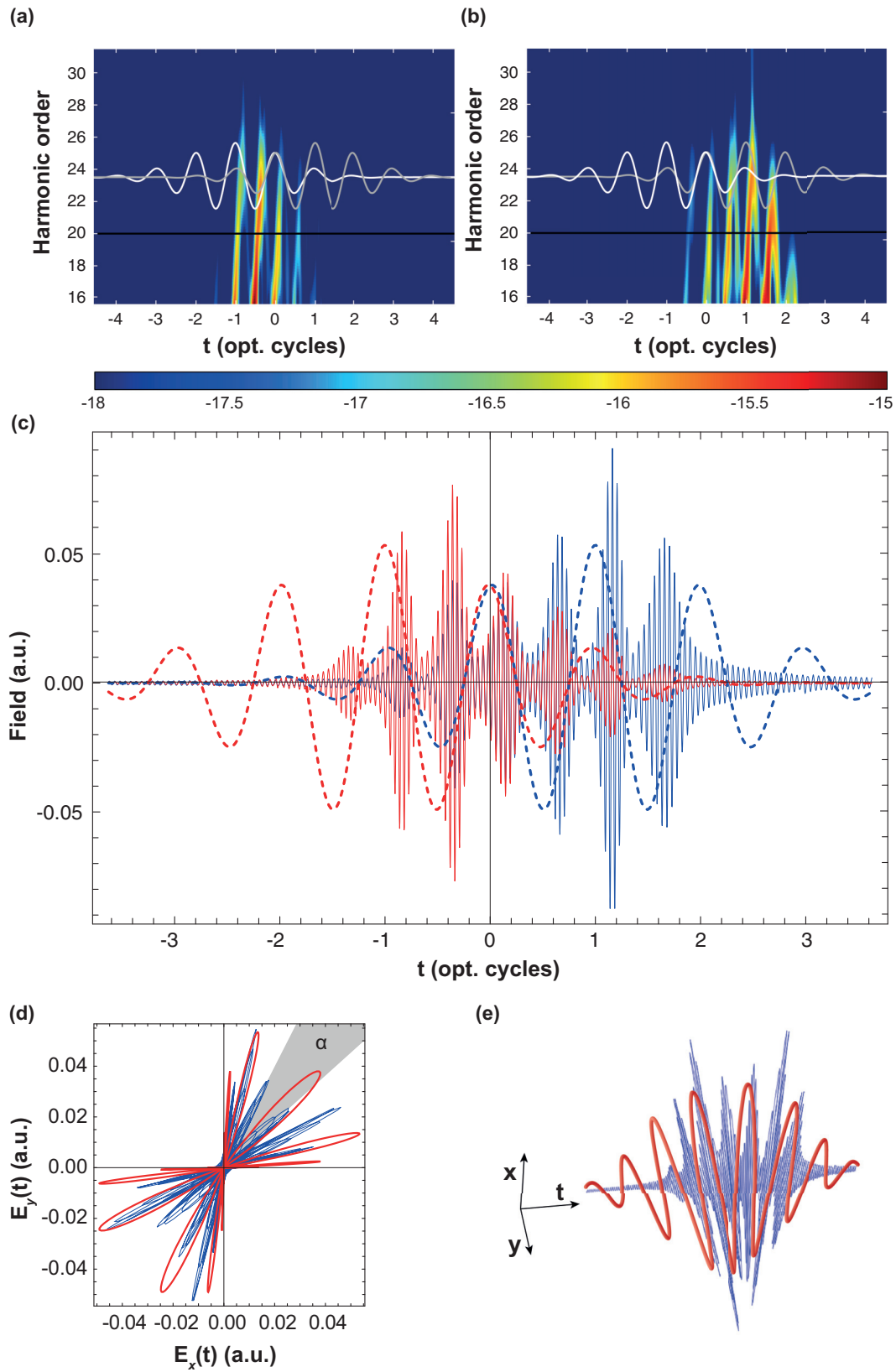


FIG. 4. Temporal anatomy of the twisted APT: few-cycle pulses version. Same as Figs. 2(c) and 2(d) [in this figure, panels (a) and (b), respectively], and Figs. 3(a)–3(c) [in this figure, panels (c)–(e), respectively], but obtained from an AP pulse with a temporal FWHM of $\Delta t = 2$ optical cycles.

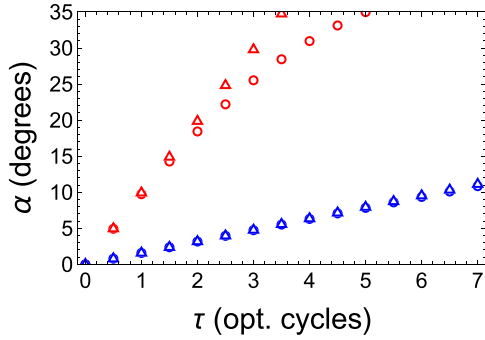


FIG. 5. Variation of the angle α as a function of the temporal delay τ . Top red (bottom blue) circles indicate the variation of the AP pulse for a temporal FWHM $\Delta t = 2$ ($\Delta t = 5$) optical cycles. For each case, the triangles show the corresponding linear approximation.

examples, we could think of several pump-probe schemes, namely, an IR pulse plus a twisted APT, an AP pulse plus a twisted APT, or a twisted APT plus a twisted APT. The latter would be an XUV pump-XUV probe scheme, but in which each of the attosecond pulses has a preferential direction in its linear polarization. In addition, because we can manipulate the polarization angle between two adjacent pulses in the APT, one can imagine sophisticated attosecond-based spectroscopy techniques using a single beam. Beyond photoelectron spectroscopy, this twisted APT can be useful to (i) study or drive highly anisotropic systems, for instance, systems where there are preferential directions, such as molecular systems, low-dimensional crystalline structures, etc. [7] and (ii) characterize multidimensional laser fields in the time domain utilizing the well-known streaking technique, mainly used for linearly polarized fields [56], among others.

Likewise, if this twisted APT are implemented in pump-probe above-threshold ionization (ATI) experiments, each of the attosecond pulses in the APT can be thought of as “isolated” by its linear polarization state, so the emitted photoelectrons would be well discriminated, angularly, with a temporal resolution of the order of attoseconds. In this sense, our technique could present advantages over other isolated attosecond pulse generation techniques. First, the possibility to work with multicycle pulses (in most of the isolated attosecond pulses generation techniques of few- or single-cycle pulses are needed). Second, the synthesis of the AP pulses is experimentally straightforward: only a single color pulse without the need for an involved interferometric system is necessary, i.e., we work in a single beam path. Third, if the spectral phase of the harmonics is compensated, for example with a metallic foil, it would be possible to use a large spectral bandwidth, generating ultrashort attosecond pulses.

Finally, let us emphasize the instrumental role of the global phase ϕ as an additional “knob” in our proposed scheme. For instance, we have proved that a change of the global phase in $\pi/2$ of the driving AP pulse echoed by a global rotation of the twisted APT. This implies that it is necessary to stabilize the global phase (carrier-envelope phase) of the AP pulse for

pump-probe experiments or if we aim for coherent control in some processes. On the contrary, this global rotation of the twisted APT can be useful to detect the change in the global phase for the AP pulse, both in the few- and multicycle regimes.

ACKNOWLEDGMENTS

M.F.C. acknowledges financial support from the Guangdong Province Science and Technology Major Project (Future functional materials under extreme conditions - 2021B0301030005) and the Guangdong Natural Science Foundation (General Program project No. 2023A1515010871). E.G.N. acknowledges to Consejo Nacional de Investigaciones Científicas y Técnicas (CONICET). F.A.V. acknowledges to Comisión de Investigaciones Científicas de la Pcia. de Buenos Aires.

APPENDIX A: PEAK AMPLITUDE OF THE SYNTHESIZED AMPLITUDE-POLARIZATION FIELD

According to the definition of amplitude-polarized (AP) electric fields (see main text) and assuming a Gaussian-shaped envelope, the explicit expressions for the components of $\mathbf{E}(t)$, when its polarization direction is at an angle of 45° , are

$$E_x(t) = E_0 e^{-2 \ln(2) \left(\frac{t+\tau/2}{\Delta t}\right)^2} \cos[\omega_0(t + \tau/2) + \phi], \quad (\text{A1a})$$

$$E_y(t) = E_0 e^{-2 \ln(2) \left(\frac{t-\tau/2}{\Delta t}\right)^2} \cos[\omega_0(t - \tau/2) + \phi]. \quad (\text{A1b})$$

In the central temporal region, i.e., around $t = 0$, the peak field amplitude $[|\mathbf{E}(t)|_{\max} = \{[E_x(t)^2 + E_y(t)^2]^{1/2}\}_{\max}]$ for such an AP pulse results in

$$|\mathbf{E}(0)|_{\max} = \sqrt{2} E_0 e^{-2 \ln(2) \left(\frac{\tau/2}{\Delta t}\right)^2}. \quad (\text{A2})$$

Therefore, when $\tau = \Delta t$, we have

$$|\mathbf{E}(0)|_{\max} = \sqrt{2} E_0 e^{-\frac{1}{2} \ln(2)} = E_0. \quad (\text{A3})$$

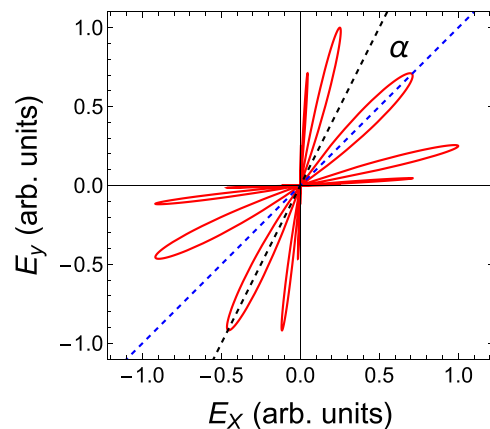


FIG. 6. Lissajous curve of the electric field of the AP pulse with a FWHM $\Delta t = 2$ optical cycles. The blue and black dashed lines indicate the angular position of the central petal and its first adjacent petal, respectively.

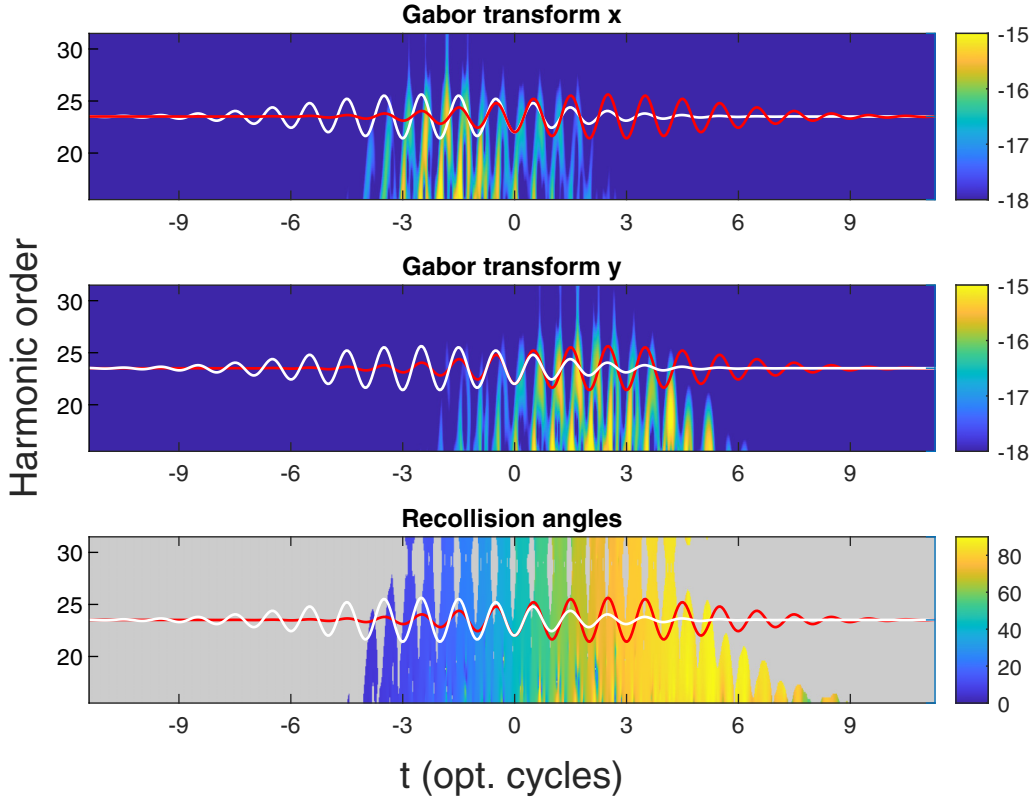


FIG. 7. Time-frequency analysis of the twisted APT: multicycle pulses version. (a), (b) Wavelet analysis obtained from the dipole accelerations $a_x(t)$ and $a_y(t)$, respectively, for an AP pulse with a temporal FWHM of $\Delta t = 5$ optical cycles. The color maps indicate the value (in log scale) of the corresponding Gabor transform $G_x(\omega, t)$ and $G_y(\omega, t)$ as a function of time and harmonic order. The x (y) component of the AP pulse is superimposed in a white (red) solid line. (c) Value of the recollision angle $\Theta(\omega, t)$ obtained from Eq. (D1). In this case, the color map scales from 0° to 90° .

APPENDIX B: NUMERICAL METHODS

To find the quantum dipole acceleration $\mathbf{a}(t) = a_x(t)\hat{e}_x + a_y(t)\hat{e}_y$, we have numerically solved the 3D-TDSE [47,48] in the dipole approximation by expanding the active electron wave function in spherical harmonics $Y_l^m(\theta, \phi)$:

$$\Psi(\mathbf{r}, t) = \sum_{l,m} \frac{R_l^m(\mathbf{r}, t)}{r} Y_l^m(\theta, \phi), \quad (\text{B1})$$

where θ and ϕ are the polar and azimuthal angles and $R_l^m(\mathbf{r}, t)$ a radial time-dependent function. Through the Ehrenfest's theorem, the x and y components of the acceleration operator $\hat{\mathbf{a}}(t)$ can be found as

$$\hat{a}_x = -[\hat{H}, [\hat{H}, \hat{x}]] = \left[\hat{H}, \frac{\partial}{\partial r} \right] \cos(\theta), \quad (\text{B2a})$$

$$\hat{a}_y = -[\hat{H}, [\hat{H}, \hat{y}]] = \left[\hat{H}, \frac{\partial}{\partial r} \right] \sin(\theta)\cos(\phi), \quad (\text{B2b})$$

where \hat{H} is the full Hamiltonian. Thus, the components of $\mathbf{a}(t)$ can be obtained as $a_x(t) = \langle \Psi(\mathbf{r}, t) | \hat{a}_x | \Psi(\mathbf{r}, t) \rangle$ and $a_y(t) = \langle \Psi(\mathbf{r}, t) | \hat{a}_y | \Psi(\mathbf{r}, t) \rangle$. The projections in the x - y plane of the harmonics spectra amplitudes $|\tilde{a}_x(\omega)|$ and $|\tilde{a}_y(\omega)|$ [Figs. 2(a)

and 2(b)], and the respective spectral phases, $\gamma_x(\omega)$ and $\gamma_y(\omega)$, are then calculated by the Fourier transforms:

$$\tilde{a}_x(\omega) = |\tilde{a}_x(\omega)| e^{i\gamma_x(\omega)} = \frac{1}{(t_f - t_i)\omega^2} \int_{t_i}^{t_f} e^{-i\omega t} a_x(t) dt, \quad (\text{B3a})$$

$$\tilde{a}_y(\omega) = |\tilde{a}_y(\omega)| e^{i\gamma_y(\omega)} = \frac{1}{(t_f - t_i)\omega^2} \int_{t_i}^{t_f} e^{-i\omega t} a_y(t) dt, \quad (\text{B3b})$$

where the times t_i and t_f define the integration window, both to solve the 3D-TDSE and to evaluate these integrals. For the first case, of the two analyzed in this work, where the FWHM of the pulse is $\Delta t = 5$ optical cycles, the numerical calculations were performed for $t_i = -2757$ a.u. and $t_f = 2757$ a.u., with a time step of 0.25 a.u. In the second case, where the FWHM of the pulse is $\Delta t = 2$ optical cycles, the integration times are $t_i = -1103$ a.u. and $t_f = 1103$ a.u., with a time step of 0.25 a.u.

Once we obtain $\mathbf{a}(t)$, a wavelet analysis can be performed by computing the Gabor transform, for both the x and y components, as follows:

$$G_{x,y}(\omega, t) = \left| \int a_{x,y}(t') \frac{\exp[-(t-t')^2/2\sigma^2]}{\sigma\sqrt{2\pi}} \exp(i\omega t') dt' \right|^2. \quad (\text{B4})$$

A value of $\sigma = 1/(3\omega_0)$ allows us to achieve an adequate balance between the time and frequency resolutions. $G_{x,y}(\omega, t)$ then gives us access to study the time dynamics behind the HHG process and compare it with classical simulations.

The x - y components of the electric field of the different APT, $E_{XUV,x}(t)$ and $E_{XUV,y}(t)$, are calculated by filtering the harmonic spectrum, and starting from the 20th ($\omega_i = 20$) harmonic order:

$$E_{XUV,x}(t) = \int_{\omega_i=20\omega_0}^{\infty} e^{i\omega t} \tilde{a}_x(\omega) d\omega, \quad (\text{B5a})$$

$$E_{XUV,y}(t) = \int_{\omega_i=20\omega_0}^{\infty} e^{i\omega t} \tilde{a}_y(\omega) d\omega. \quad (\text{B5b})$$

APPENDIX C: LISSAJOUS CURVES OF THE IR-AP PULSE AND ANGLE BETWEEN TWO ADJACENT PETALS

In this Appendix, we describe how the angle α between two adjacent petals in the Lissajous curves of the driving AP field varies as a function of the temporal delay τ . The importance of this angle lies in the fact that it represents the angular difference between the polarization directions of two adjacent attosecond pulses in the twisted APT, near the center of the temporal region.

Figure 6 shows the Lissajous curve of the electric field of an AP pulse whose temporal FWHM is $\Delta t = 2$ optical cycles. In this figure, α corresponds to the angular separation between the black and blue dashed lines. The blue dashed line intersects the position of the maximum field amplitude at 45°

(global phase $\phi = 0$) while the black dashed line intersects the position of the adjacent maximum. Mathematically, we can find the angle α after evaluating the field $\mathbf{E}(t)$ at $t = 1/2$ optical cycle, which corresponds to the temporal position of the petal indicated by the black dashed line in the figure and taking the angular distance to the angle $\pi/4$, which gives the position of the central petal at $t = 0$:

$$\begin{aligned} \alpha(t = 1/2, \tau, \Delta t) &= \tan^{-1} \left(\frac{E_x(1/2)}{E_y(1/2)} \right) - \frac{\pi}{4} \\ &= \tan^{-1} \left(\frac{e^{-2 \ln(2) \left(\frac{1/2 - \tau/2}{\Delta t} \right)^2}}{e^{-2 \ln(2) \left(\frac{1/2 + \tau/2}{\Delta t} \right)^2}} \right) - \frac{\pi}{4} \\ &= \frac{\ln(2)\tau}{\Delta t^2} + O(\tau^2). \end{aligned} \quad (\text{C1})$$

Equation (C1) indicates that α can mathematically take any value between zero and $\pi/4$, increasing as the ratio $\tau/\Delta t$ increases. Moreover, as we showed in Appendix A [Eqs. (A2) and (A3)], the peak field amplitude of the AP driving pulse, at $t = 0$, reaches its maximum value, $|\mathbf{E}(0)|_{\max} = E_0$, for $\tau = \Delta t$, while for $\tau > \Delta t$ it is $|\mathbf{E}(0)|_{\max} < E_0$. Therefore, since the HHG requires that the amplitude of the driving field is enough to reach the tunnel ionization condition, the maximum value of angular separation between two consecutive attosecond pulses, which is possible to achieve experimentally, will depend on the atomic species considered as the target.

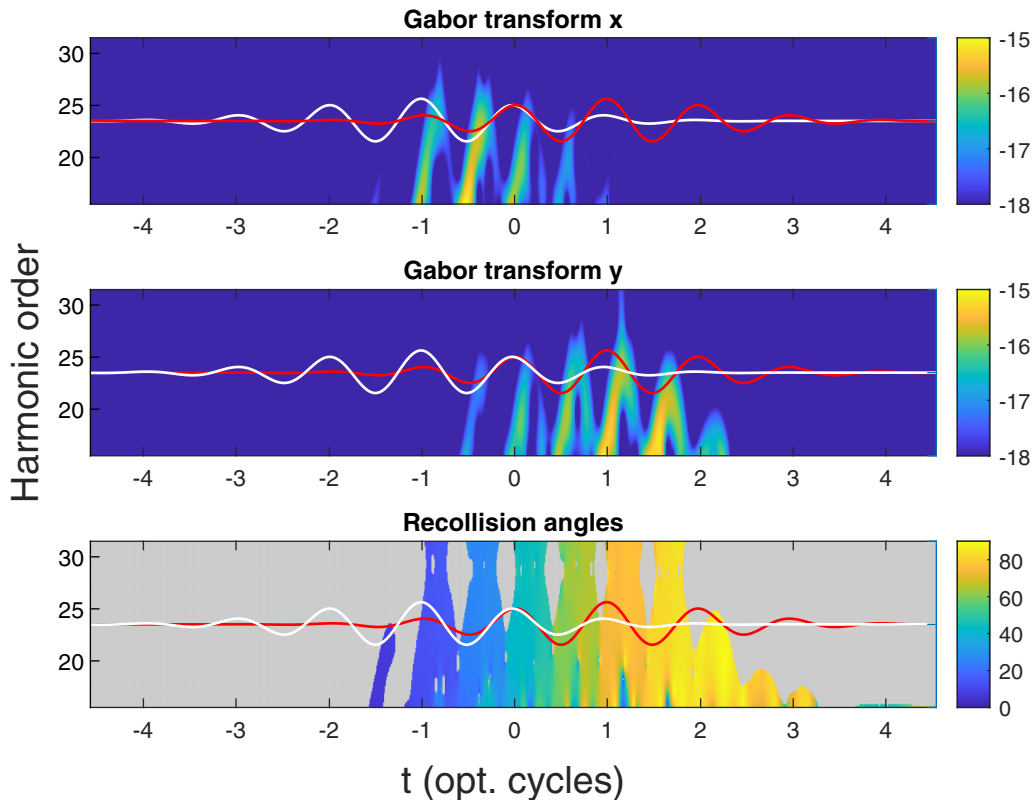


FIG. 8. Time-frequency analysis of the twisted APT: few-cycle pulses version. Same as Fig. 7 but for an AP pulse with a temporal FWHM of $\Delta t = 2$ optical cycles.

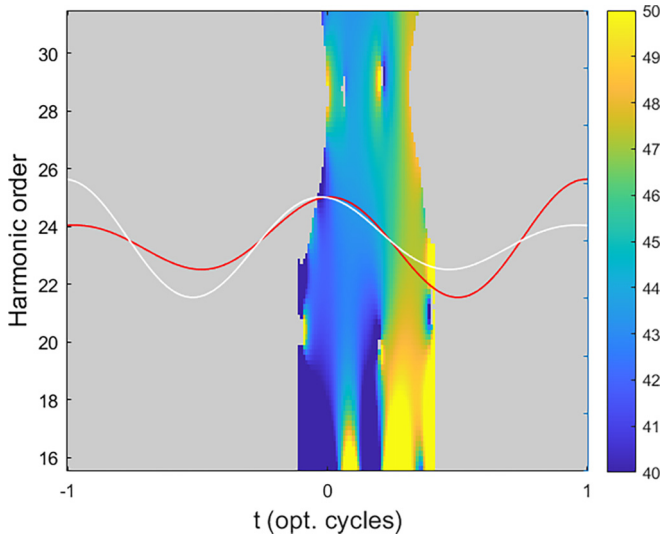


FIG. 9. Time-frequency analysis of a single burst of the few-cycle pulse. Recollision angles obtained from Eq. (D1) for a single burst, approximately, between zero and 0.5 optical cycles, where the x (y) component of the AP pulse (same AP pulse that was considered for the analysis in Fig. 8) is superimposed in white (red) solid line. The color map scales from 40° to 50° .

It is worth mentioning that, for ultrashort pulses in the sub-two-cycle regime, the temporal position at $t = 1/2$ optical cycle is not well described by $T_0 \equiv 2\pi/\omega_0$ but by the *principal period* $T_P \equiv 2\pi/\omega_P$, where ω_P refers to the *principal frequency* (see Refs. [57,58] for definition and in-depth analysis of these concepts). This is the period (frequency) that allows us to correctly locate the position of the maxima field amplitude for such ultrashort pulses. Also, it should be noted that the angle α results τ -independent when τ is an integer multiple of T_0 . Here, the AP pulse has right or left polarization (see main text for more details).

APPENDIX D: TIME-RESOLVED RECOLLISION ANGLES

From the results of the time-frequency analysis using the Gabor transform (see Appendix B), here we calculate the

time-resolved recollision angle of ionized electrons [47]. This quantity can be derived as

$$\Theta(\omega, t) = \tan^{-1} \left(\sqrt{\frac{G_y(\omega, t)}{G_x(\omega, t)}} \right), \quad (\text{D1})$$

where we restrict ourselves to the first quadrant, i.e., $\Theta(\omega, t) > 0$. This angle determines the angle at which the electron recombines with its parent ion.

The complete wavelet analysis can be seen in Fig. 7, where we show the results for an AP pulse with a temporal FWHM of $\Delta t = 5$ optical cycles and a global phase $\phi = 0$. Figures 7(a) and 7(b) depict the color maps of the Gabor transforms for the associated HHG spectrum, $G_x(\omega, t)$ and $G_y(\omega, t)$, while the color map in Fig. 7(c) indicates the corresponding value of $\Theta(\omega, t)$. It is worth mentioning that values of $\Theta(\omega, t)$ above, approximately, the 28th harmonic order, have no physical meaning since the emission probability is negligible [they are numerical artifacts that come from the computation of the expression in Eq. (D1)]. From Fig. 7(c), we can observe how the variation of the emission angle between the different bursts of XUV radiation is, which indicates the polarization angle of the different attosecond pulses in the APT. In agreement with what is seen in the main text, this angle goes from 0° to 90° , indicating the rotation of the polarization of the AP pulse in the x - y plane.

Figure 8 shows the analysis analogous to the one performed in Fig. 7, but for the case of an AP pulse with $\Delta t = 2$ optical cycles. In Fig. 8(c), it can be seen the variation of the emission angle between the different bursts of XUV radiation, or attosecond pulses, which, as expected, is greater than in the previous case.

Finally, in Fig. 9, we show the variation of the emission angle for a single burst which is generated, approximately, between zero optical cycles and 0.5 optical cycles. From this figure, it can be observed the angle of the recombination for the short and long trajectories in a single burst, or in a half laser cycle. Between the 16th and the 20th harmonic order, the short trajectories recombine with an angle of 40° , while the long trajectories do so at an angle of 50° . Above the 20th harmonic order (cutoff region), the angle of recombination of both trajectories converges, approximately, to 45° .

-
- [1] F. Krausz and M. Ivanov, Attosecond physics, *Rev. Mod. Phys.* **81**, 163 (2009).
- [2] F. Krausz, The birth of attosecond physics and its coming of age, *Phys. Scr.* **91**, 063011 (2016).
- [3] P.-M. Paul, E. S. Toma, P. Breger, G. Mullot, F. Augé, P. Balcou, H. G. Muller, and P. Agostini, Observation of a train of attosecond pulses from high harmonic generation, *Science* **292**, 1689 (2001).
- [4] G. Sansone, E. Benedetti, F. Calegari, C. Vozzi, L. Avaldi, R. Flammini, L. Poletto, P. Villoresi, C. Altucci, R. Velotta *et al.*, Isolated single-cycle attosecond pulses, *Science* **314**, 443 (2006).
- [5] M. T. Hassan, T. T. Luu, A. Moulet, O. Raskazovskaya, P. Zhokhov, M. Garg, N. Karpowicz, A. Zheltikov, V. Pervak, F. Krausz *et al.*, Optical attosecond pulses and tracking the nonlinear response of bound electrons, *Nature (London)* **530**, 66 (2016).
- [6] F. Krausz and M. I. Stockman, Attosecond metrology: From electron capture to future signal processing, *Nat. Photonics* **8**, 205 (2014).
- [7] J. Li, J. Lu, A. Chew, S. Han, J. Li, Y. Wu, H. Wang, S. Ghimire, and Z. Chang, Attosecond science based on high harmonic generation from gases and solids, *Nat. Commun.* **11**, 1 (2020).
- [8] K. Midorikawa, Progress on table-top isolated attosecond light sources, *Nat. Photonics* **16**, 267 (2022).
- [9] K. Amini, J. Biegert, F. Calegari, A. Chacón, M. F. Ciappina, A. Dauphin, D. K. Efimov, C. F. de Morisson Faria, K. Giergiel, P.

- Gniewek *et al.*, Symphony on strong field approximation, *Rep. Prog. Phys.* **82**, 116001 (2019).
- [10] H. Timmers, M. Sabbar, J. Hellwagner, Y. Kobayashi, D. M. Neumark, and S. R. Leone, Polarization-assisted amplitude gating as a route to tunable, high-contrast attosecond pulses, *Optica* **3**, 707 (2016).
- [11] F. Calegari, G. Sansone, S. Stagira, C. Vozzi, and M. Nisoli, Advances in attosecond science, *J. Phys. B: At., Mol. Opt. Phys.* **49**, 062001 (2016).
- [12] K. Misawa, Applications of polarization-shaped femtosecond laser pulses, *Adv. Phys.: X* **1**, 544 (2016).
- [13] A. M. Weiner, Ultrafast optical pulse shaping: A tutorial review, *Opt. Commun.* **284**, 3669 (2011).
- [14] Y. Shen, Q. Zhan, L. G. Wright, D. N. Christodoulides, F. W. Wise, A. E. Willner, Z. Zhao, K.-h. Zou, C.-T. Liao, C. Hernández-García *et al.*, Roadmap on spatiotemporal light fields, *J. Opt.* **25**, 093001 (2023).
- [15] C. Hernández-García, A. Picón, J. San Román, and L. Plaja, Attosecond extreme ultraviolet vortices from high-order harmonic generation, *Phys. Rev. Lett.* **111**, 083602 (2013).
- [16] R. Géneaux, A. Camper, T. Auguste, O. Gobert, J. Caillat, R. Taïeb, and T. Ruchon, Synthesis and characterization of attosecond light vortices in the extreme ultraviolet, *Nat. Commun.* **7**, 12583 (2016).
- [17] L. Rego, K. M. Dorney, N. J. Brooks, Q. L. Nguyen, C.-T. Liao, J. San Román, D. E. Couch, A. Liu, E. Pisanty, M. Lewenstein *et al.*, Generation of extreme-ultraviolet beams with time-varying orbital angular momentum, *Science* **364**, eaaw9486 (2019).
- [18] B. Minneker, B. Böning, A. Weber, and S. Fritzsche, Torusknot angular momentum in twisted attosecond pulses from high-order harmonic generation, *Phys. Rev. A* **104**, 053116 (2021).
- [19] Y. Fang, S. Lu, and Y. Liu, Controlling photon transverse orbital angular momentum in high harmonic generation, *Phys. Rev. Lett.* **127**, 273901 (2021).
- [20] O. Neufeld and O. Cohen, Optical chirality in nonlinear optics: Application to high harmonic generation, *Phys. Rev. Lett.* **120**, 133206 (2018).
- [21] P.-C. Huang, C. Hernández-García, J.-T. Huang, P.-Y. Huang, C.-H. Lu, L. Rego, D. D. Hickstein, J. L. Ellis, A. Jaron-Becker, A. Becker *et al.*, Polarization control of isolated high-harmonic pulses, *Nat. Photonics* **12**, 349 (2018).
- [22] J. Wätzel and J. Berakdar, Multipolar, polarization-shaped high-order harmonic generation by intense vector beams, *Phys. Rev. A* **101**, 043409 (2020).
- [23] D. B. Milošević and W. Becker, Attosecond pulse trains with unusual nonlinear polarization, *Phys. Rev. A* **62**, 011403(R) (2000).
- [24] D. B. Milošević, W. Becker, and R. Kopold, Generation of circularly polarized high-order harmonics by two-color coplanar field mixing, *Phys. Rev. A* **61**, 063403 (2000).
- [25] A. Fleischer, O. Kfir, T. Diskin, P. Sidorenko, and O. Cohen, Spin angular momentum and tunable polarization in high-harmonic generation, *Nat. Photonics* **8**, 543 (2014).
- [26] O. Kfir, P. Grychtol, E. Turgut, R. Knut, D. Zusin, D. Popmintchev, T. Popmintchev, H. Nembach, J. M. Shaw, A. Fleischer *et al.*, Generation of bright phase-matched circularly-polarized extreme ultraviolet high harmonics, *Nat. Photonics* **9**, 99 (2015).
- [27] L. Rego, J. San Román, L. Plaja, and C. Hernández-García, Trains of attosecond pulses structured with time-ordered polarization states, *Opt. Lett.* **45**, 5636 (2020).
- [28] Á. Jiménez-Galán, G. Dixit, S. Patchkovskii, O. Smirnova, F. Morales, and M. Ivanov, Attosecond recorder of the polarization state of light, *Nat. Commun.* **9**, 850 (2018).
- [29] K. M. Dorney, J. L. Ellis, C. Hernández-García, D. D. Hickstein, C. A. Mancuso, N. Brooks, T. Fan, G. Fan, D. Zusin, C. Gentry *et al.*, Helicity-selective enhancement and polarization control of attosecond high harmonic waveforms driven by bichromatic circularly polarized laser fields, *Phys. Rev. Lett.* **119**, 063201 (2017).
- [30] Á. Jiménez-Galán, N. Zhavoronkov, D. Ayuso, F. Morales, S. Patchkovskii, M. Schloz, E. Pisanty, O. Smirnova, and M. Ivanov, Control of attosecond light polarization in two-color bicircular fields, *Phys. Rev. A* **97**, 023409 (2018).
- [31] D. B. Milošević, Control of the helicity of high-order harmonics generated by bicircular laser fields, *Phys. Rev. A* **98**, 033405 (2018).
- [32] A. Fleischer, E. Bordo, O. Kfir, P. Sidorenko, and O. Cohen, Polarization-fan high-order harmonics, *J. Phys. B: At., Mol. Opt. Phys.* **50**, 034001 (2017).
- [33] A. D. Bandrauk, J. Guo, and K.-J. Yuan, Circularly polarized attosecond pulse generation and applications to ultrafast magnetism, *J. Opt. (Bristol, UK)* **19**, 124016 (2017).
- [34] G. Lambert, B. Vodungbo, J. Gautier, B. Mahieu, V. Malka, S. Sebban, P. Zeitoun, J. Luning, J. Perron, A. Andreev *et al.*, Towards enabling femtosecond helicity-dependent spectroscopy with high-harmonic sources, *Nat. Commun.* **6**, 6167 (2015).
- [35] K.-J. Yuan and A. D. Bandrauk, Attosecond-magnetic-field-pulse generation by intense few-cycle circularly polarized UV laser pulses, *Phys. Rev. A* **88**, 013417 (2013).
- [36] T. Fan, P. Grychtol, R. Knut, C. Hernández-García, D. D. Hickstein, D. Zusin, C. Gentry, F. J. Dollar, C. A. Mancuso, C. W. Hogle *et al.*, Bright circularly polarized soft x-ray high harmonics for x-ray magnetic circular dichroism, *Proc. Natl. Acad. Sci. USA* **112**, 14206 (2015).
- [37] D. B. Milošević, Circularly polarized high harmonics generated by a bicircular field from inert atomic gases in the p state: A tool for exploring chirality-sensitive processes, *Phys. Rev. A* **92**, 043827 (2015).
- [38] C. Chen, Z. Tao, C. Hernández-García, P. Matyba, A. Carr, R. Knut, O. Kfir, D. Zusin, C. Gentry, P. Grychtol *et al.*, Tomographic reconstruction of circularly polarized high-harmonic fields: 3D attosecond metrology, *Sci. Adv.* **2**, e1501333 (2016).
- [39] G. Karras, M. Ndong, E. Hertz, D. Sugny, F. Billard, B. Lavorel, and O. Faucher, Polarization shaping for unidirectional rotational motion of molecules, *Phys. Rev. Lett.* **114**, 103001 (2015).
- [40] I. Tutunnikov, E. Gershnel, S. Gold, and I. S. Averbukh, Selective orientation of chiral molecules by laser fields with twisted polarization, *J. Phys. Chem. Lett.* **9**, 1105 (2018).
- [41] H. Yuan, L. He, S. M. Njoroge, D. Wang, R. Shao, P. Lan, and P. Lu, Generation of near-circularly polarized attosecond pulse with tunable helicity by unidirectionally rotating laser field, *Ann. Phys. (Berlin, Ger.)* **532**, 1900570 (2020).

- [42] K. Lin, I. Tutunnikov, J. Ma, J. Qiang, L. Zhou, O. Faucher, Y. Prior, I. S. Averbukh, and J. Wu, Spatiotemporal rotational dynamics of laser-driven molecules, *Adv. Photonics* **2**, 024002 (2020).
- [43] S. Pan, C. Hu, Z. Zhang, P. Lu, C. Lu, L. Zhou, J. Wang, F. Sun, J. Qiang, H. Li *et al.*, Low-energy protons in strong-field dissociation of H_2^+ via dipole-transitions at large bond lengths, *Ultrafast Sci.* **2022**, 9863548 (2022).
- [44] E. Prost, E. Hertz, F. Billard, B. Lavorel, and O. Faucher, Polarization-based tachometer for measuring spinning rotors, *Opt. Express* **26**, 31839 (2018).
- [45] L. Xu, I. Tutunnikov, L. Zhou, K. Lin, J. Qiang, P. Lu, Y. Prior, I. S. Averbukh, and J. Wu, Echoes in unidirectionally rotating molecules, *Phys. Rev. A* **102**, 043116 (2020).
- [46] Q. Ji, S. Pan, P. He, J. Wang, P. Lu, H. Li, X. Gong, K. Lin, W. Zhang, J. Ma *et al.*, Timing dissociative ionization of H_2 using a polarization-skewed femtosecond laser pulse, *Phys. Rev. Lett.* **123**, 233202 (2019).
- [47] M. Murakami, O. Korobkin, and M. Horbatsch, High-harmonic generation from hydrogen atoms driven by two-color mutually orthogonal laser fields, *Phys. Rev. A* **88**, 063419 (2013).
- [48] M. Murakami, O. Korobkin, and M. Horbatsch, High-harmonic generation from hydrogen atoms driven by two-color mutually orthogonal laser fields, *Phys. Rev. A* **95**, 059909(E) (2017).
- [49] E. Gustafsson, T. Ruchon, M. Swoboda, T. Remetter, E. Pourtal, R. López-Martens, P. Balcou, and A. L'Huillier, Broadband attosecond pulse shaping, *Opt. Lett.* **32**, 1353 (2007).
- [50] M. Chini, K. Zhao, and Z. Chang, The generation, characterization and applications of broadband isolated attosecond pulses, *Nat. Photonics* **8**, 178 (2014).
- [51] W. Jiang, G. S. Armstrong, J. Tong, Y. Xu, Z. Zuo, J. Qiang, P. Lu, D. D. A. Clarke, J. Benda, A. Fleischer *et al.*, Atomic partial wave meter by attosecond coincidence metrology, *Nat. Commun.* **13**, 5072 (2022).
- [52] X. Gong, W. Jiang, J. Tong, J. Qiang, P. Lu, H. Ni, R. Lucchese, K. Ueda, and J. Wu, Asymmetric attosecond photoionization in molecular shape resonance, *Phys. Rev. X* **12**, 011002 (2022).
- [53] D. Busto, J. Vinbladh, S. Zhong, M. Isinger, S. Nandi, S. Maclot, P. Johnsson, M. Gisselbrecht, A. L'Huillier, E. Lindroth *et al.*, Fano's propensity rule in angle-resolved attosecond pump-probe photoionization, *Phys. Rev. Lett.* **123**, 133201 (2019).
- [54] S. Beaulieu, A. Comby, A. Clergerie, J. Caillat, D. Descamps, N. Dudovich, B. Fabre, R. Géneaux, F. Légaré, S. Petit *et al.*, Attosecond-resolved photoionization of chiral molecules, *Science* **358**, 1288 (2017).
- [55] J. Joseph, F. Holzmeier, D. Bresteau, C. Spezzani, T. Ruchon, J. Hergott, O. Tcherbakoff, P. D'Oliveira, J. Houver, and D. Doweck, Angle-resolved studies of XUV-IR two-photon ionization in the RABBITT scheme, *J. Phys. B: At., Mol. Opt. Phys.* **53**, 184007 (2020).
- [56] E. Goulielmakis, M. Uiberacker, R. Kienberger, A. Baltuska, A. S. V. Yakovlev, T. Westerwalbesloh, U. Kleineberg, U. Heinzmann, M. Drescher, and F. Krausz, Direct measurement of light waves, *Science* **305**, 1267 (2004).
- [57] E. G. Neyra, P. Vaveliuk, E. Pisanty, A. S. Maxwell, M. Lewenstein, and M. F. Ciappina, Principal frequency of an ultrashort laser pulse, *Phys. Rev. A* **103**, 053124 (2021).
- [58] E. G. Neyra, D. A. Biasetti, F. Videla, L. Rebón, and M. F. Ciappina, Principal frequency, superbandwidth, and low-order harmonics generated by superoscillatory pulses, *Phys. Rev. Res.* **4**, 033254 (2022).